Supporting Information:

Electrochemical Synthesis of Individual Core@Shell and Hollow Ag/Ag_2S Nanoparticles

Donald A. Robinson and Henry S. White.*

Department of Chemistry, University of Utah, Salt Lake City, UT 84112, United States

*Corresponding author: white@chem.utah.edu

Contents

S1. Experimental methods

A. Materials

Water used for rinsing and preparing solutions was purified using a Smart2Pure 12 UV/UF water purification system (Thermoscientific), resistivity of 18.2 MΩ·cm. Citrate-stabilized Ag nanoparticles of quasispherical shape, 68±8 nm diameter, were purchased from nanoComposix, Inc. The stock solution contained 0.91 nM Ag nanoparticles (5.5×10^{11} particles/mL) in 2 mM sodium citrate buffer, pH 7.5. Sodium hydroxide (NaOH) and sodium sulfide (Na_2S) pellets were obtained from Fisher Scientific. Potassium phthalate monobasic (KHP, ACS reagent), potassium ferrocyanide, potassium nitrate (KNO_3), and perchloric acid ($HClO_4$, ACS reagent, 70%) were purchased from Sigma-Aldrich. Vials equipped with PTFE/silicone septum caps were purchased from ThermoFisher Scientific (catalog no. C4015-492). TEM sample grids were procured from Ted Pella, Inc. Imaging of Ag NPs was performed using Cu TEM grids coated with lacey carbon film (product no. 01824) and ex-situ electrochemical $Ag@Ag_2S$ NP synthesis experiments were performed using Au TEM grids coated with 2-3 nm Au films (Substratek™, product no. 21420-25) as the working electrodes (see Section S1-E).

B. Electrochemical instrumentation

All electrochemical measurements employed a "leakless" Ag/AgCl reference electrode (3.5 M KCl, eDAQ Pty. Ltd., catalog no. ET072-1). Potentials are reported as overpotentials versus the reversible potential for Ag/Ag_2S (measured as -0.74 V vs the "leakless" Ag/AgCl reference electrode).

Electrochemical measurements at Ag macroelectrodes and TEM grid electrodes were performed using a CHI 760E bipotentiostat (CH instruments) configured with Picoamp booster preamplifier (CHI 201, CH instruments) and a 3-electrode cell (Pt counter electrode) housed in a Faraday cage.

Amperometric measurements of Ag NP collisions/oxidations were acquired using a Chem-Clamp voltammeter-amperometer (Dagan Corporation). The 3-pole low-pass Bessel filter of the Chem-Clamp amplifier was set to 10 kHz with a 10 mV/pA gain setting. The electrode potential was controlled using a Pine bipotentiostat (Model AFRDE5) as a waveform generator. Data were acquired at a 50 kHz sampling using a PCI-6251 data acquisition card (National Instruments) and a custom LabVIEW virtual interface.

C. Ag→Ag_2S nanoparticle collisions at Au microelectrode

Prior to performing a new Ag nanoparticle collision measurement, a Au microdisk working electrode, 12.5 μm diameter (CH Instruments), was mechanically polished using Microcut® discs, 1200 grit (Buehler, ITW, Inc), subsequently polished using a slurry of alumina particles (~50 nm grain size) on a microcloth (Buehler, ITW, Inc), then cleaned on a separate wetted microcloth, rinsing with copious water in between each polishing/cleaning step. The Au microelectrode was then cycled in 0.1 M $HClO_4$ between -0.8 and 1.2 V vs $Hg/HgSO_4$ reference electrode (sat K_2SO_4, CH Instruments) at a scan rate of 100 mV/s until a reproducible voltammogram was obtained. A stock solution of NaOH was prepared and standardized by KHP titration using a Mettler Toledo™ FE20 FiveEasy™ pH meter. The concentration of the NaOH stock solution was determined to be 0.14 M. A solution of 1 mM Na_2S was freshly prepared on the day of a new electrochemical experiment.

The sample preparation procedure for Ag NP collision measurements is shown schematically in Figure S1. The procedure was designed to prevent the O_2-driven chemical transformation of Ag NPs to Ag_2S.[1-2] First, a 108 μL aliquot of 0.14 M NaOH and a 15 μL aliquot of 0.1 M Na_2S were added to a 2 mL vial containing 1362 μL of water. This solution was then bubbled with Ar gas for 10 min, maintaining a gas-tight seal using a PTFE/silicone septum cap. A needle for gas outlet and the reference electrode were also inserted through the septum. Meanwhile, the stock solution of Ag NPs was also bubbled with Ar gas for 10 min. A 15 μL aliquot of the pre-purged Ag NP stock solution was quickly extracted and delivered to the Na_2S solution while maintaining Ar bubbling (Figure S1). To accomplish this, a plastic pipette tip was modified by cutting with scissors and repurposed as an injection port to allow a smaller pipet tip to deliver the Ag NP solution using an Eppendorf pipette. The injection port was then removed, and the hole in the septum was used to insert a Au disk microelectrode (12.5 μm diameter, CH instruments), all while maintaining Ar bubbling. The final solution contained 9 pM Ag NPs, 1 mM Na_2S, and 10 mM NaOH, pH 12. After injection of Ag NPs, the gas outlet needle was removed and the Ar inlet tubing was raised above the solution/gas interface to maintain inert gas atmosphere during single-nanoparticle measurements (Figure S1b).

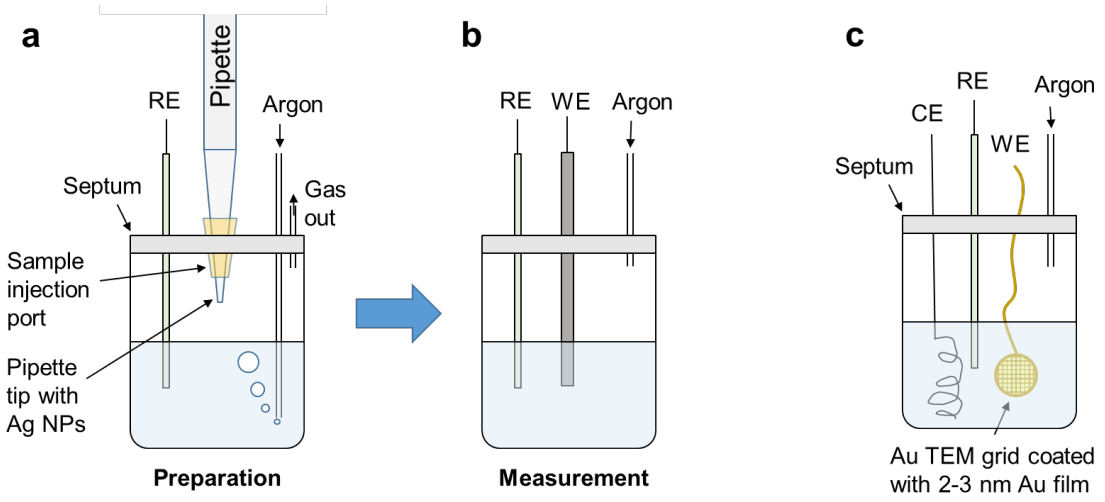

Figure S1. Schematic showing sample preparation and electrochemical setup for **(a/b)** measurement of individual Ag nanoparticle collisions at a Au microelectrode, WE, and **(c)** electrochemical cell for performing anodic Ag@Ag_2S NP synthesis at Au-coated TEM grid. RE: reference electrode, WE: working electrode, CE: counter electrode.

D. Ag→Ag_2S transformation at Ag NPs deposited via dropcast at Au microelectrode

A 1 µL drop of the Ag NP stock solution was deposited on the surface of a 12.5 µm diameter Au disk electrode and allowed to evaporate. Cyclic voltammetry was then performed at the AgNP-modified electrode in a dearrated solution containing 1 mM Na_2S and 10 mM NaOH (Figure S4).

E. Ag nanoparticle collisions at Au-coated TEM grid electrodes

As shown in Figure S1c, a similar procedure as described above was used to drive anodic formation of Ag@Ag_2S NPs at a Au film-coated TEM sample grid (WE), with the inclusion of a coiled Pt wire to serve as the counter electrode (CE). For TEM grid electrode fabrication, a 25 µm diameter Au wire (Alpha-Aesar) was threaded through the punch-out in the shape of the number 1 at the edge of the grid, and tied around the edge of the grid, as guided by an optical microscope and delicately handled with tweezers/clamps. The excess Au wire was then wrapped tightly around a tungsten wire. The electrical resistance was tested using a multimeter, attaching one lead to the TEM grid by metallic tweezers and the other to the tungsten wire. Figure S2 shows cyclic voltammetry of ferrocyanide, $[Fe(CN)_6]^{4-}$, at a Au-coated TEM grid, thus demonstrating its functionality as an electrode.

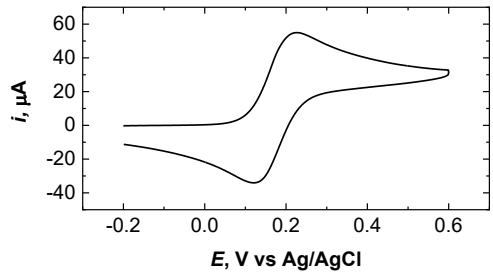

Figure S2. Cyclic voltammogram for 5 mM $[Fe(CN)_6]^{4-}$ at Au-coated TEM grid, 0.5 M KNO_3 supporting electrolyte, 20 mV s^{-1} scan rate.

After setting up the cell in Figure S1c, a potential was applied to the TEM grid for 10 min. Immediately afterwards, the grid was lifted out of solution and left to dry under the protection of Ar gas. While maintaining an Ar blanket, the solution was extracted using an air-tight syringe (Hamilton Co., Gastight® 1010) that was backfilled with Ar gas prior to extraction. A deaerated solution of 10 mM NaOH was then injected in the sealed vial and the TEM grid was immersed in to the solution to rinse away residual salts. After 30 min of soaking, this solution was extracted and replaced with deaerated purified water following a similar protocol as described above. After another 30 min of soaking, the water was extracted and the grid was allowed to dry under Ar atmosphere.

F. Electron microscopy

Electron microscopy and element mapping were performed using a JEOL JEM-2800 scanning transmission electron microscope (S/TEM) equipped with a dual detector energy-dispersive x-ray spectrometer (EDX), operated at 200 kV accelerating voltage.

F. Signal processing and analysis of current transients

The raw *i-t* data were post-filtered with Matlab by a previously described method.[3] Briefly, a digital translation of a low-pass Bessel filter, available online for public use,[4-5] was used to optimize signal-to-noise without sacrificing temporal resolution. Maximum currents (i_{max}), event durations (Δt), and charges (Q) were measured using the "Peak Analysis" module of OriginPro 2018b. Baselines were fitted using the median current, making sure that the selected data analysis window containing the current transient being measured included at least 5,000 data points of flat background current to achieve an accurate baseline for integration. Statistical analysis was also performed using OriginPro 2018b.

S2. Voltammetry of Ag/Ag_2S reaction at bare and Ag nanoparticle-modified Au microelectrodes

Figure S3 shows a voltammogram for the anodic oxidation of HS^- to form S adlayers on the Au surface.[6] Anodic peaks correspond to S adlayer formation and cathodic peaks represent the reduction to adsorbed sulfides, which render the surface more catalytically active for the hydrogen evolution reaction[7] as the potential is swept negative of -0.4 V. At potentials positive of the selected window, the formation of sulfur and polysulfide multilayers occurs,[6] which would interfere with nanoparticle adsorption and reaction kinetics. Therefore, 0.35 V was chosen as the maximum potential applied in single-nanoparticle measurements.

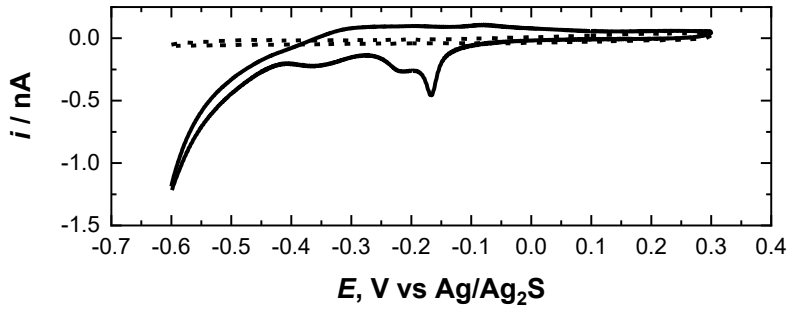

Figure S3. Cyclic voltammogram of S adlayer formation at a 12.5 µm diameter Au microelectrode, 100 mV s^{-1} scan rate. The deaerated solution contains 1 mM Na_2S and 10 mM NaOH. Dashed trace represents a control without any added Na_2S.

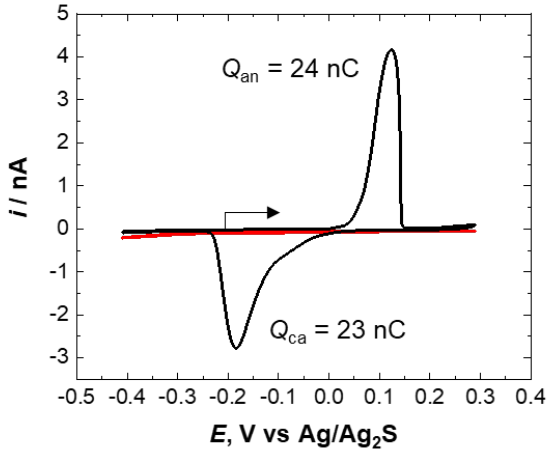

Figure S4. Cyclic voltammogram of electrochemical sulfidation at 70 nm diameter Ag nanoparticles deposited by dropcasting on a 12.5 µm diameter Au microelectrode, 5 mV s^{-1} scan rate. The deaerated solution contains 1 mM Na_2S and 10 mM NaOH. Red trace shows voltammetry for a control for the bare electrode without deposited nanoparticles. Black arrow marks the start of the initial positive potential sweep. Values of the charge measured by integration of the anodic and cathodic peaks are labelled on the plot as Q_{an} and Q_{ca}, respectively.

S3. Additional examples of single-nanoparticle electrochemical sulfidation transients

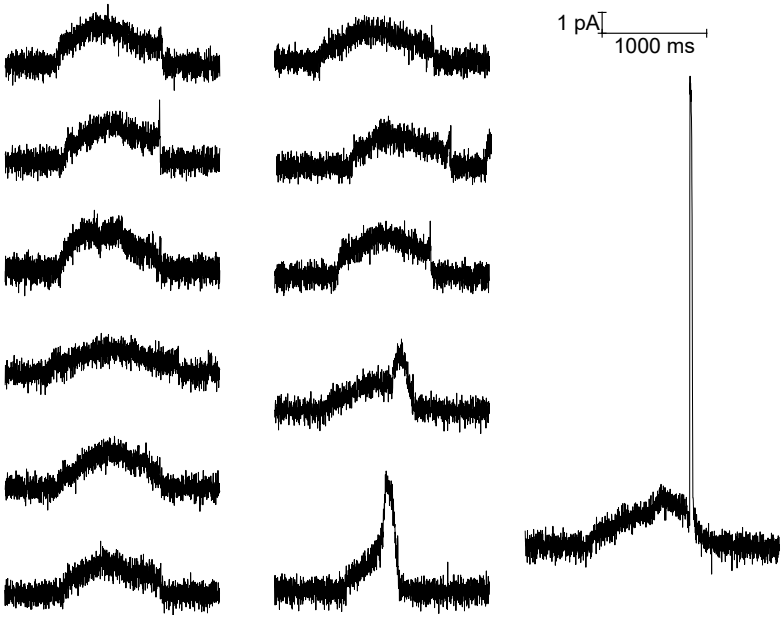

Figure S5. Representative current transients for single-nanoparticle sulfidation at 50 mV overpotential. Solution conditions and filter/acquisition rate are similar to those described in Figure 1 caption of the main text.

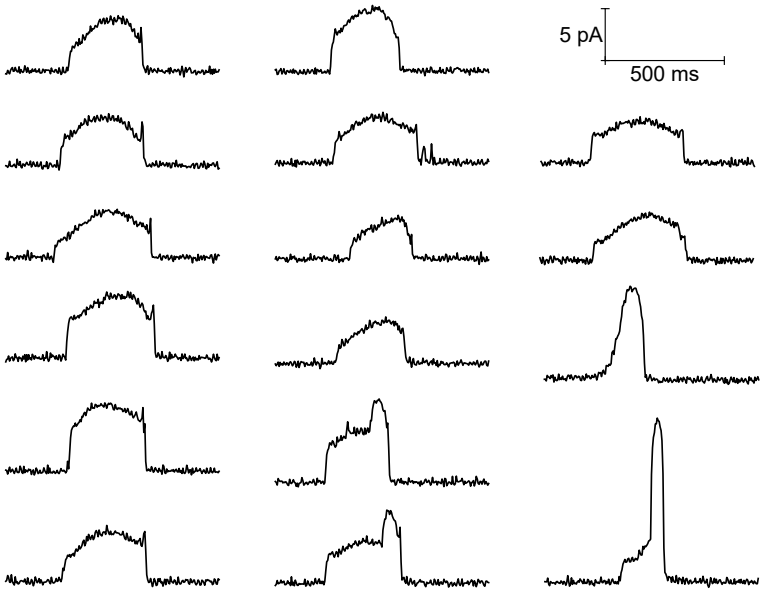

Figure S6. Representative current transients for single-nanoparticle sulfidation at 100 mV overpotential. Solution conditions and filter/acquisition rate are similar to those described in Figure 1 caption of the main text.

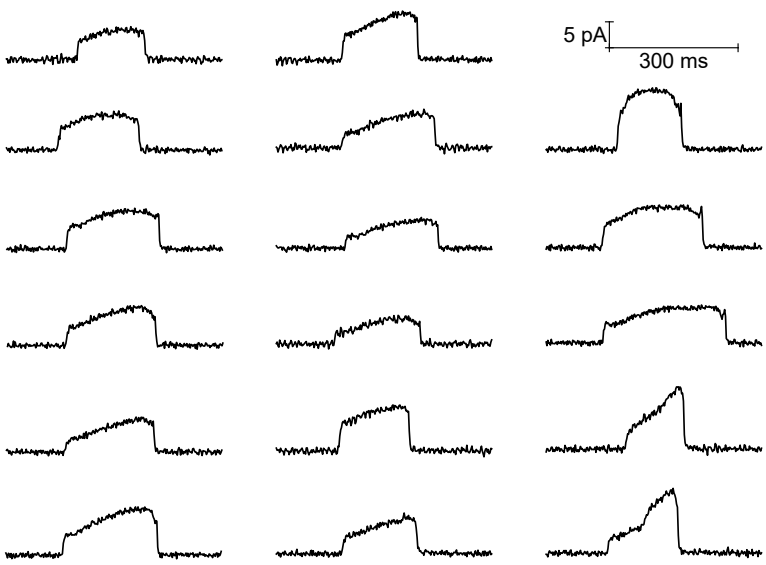

Figure S7. Representative current transients for single-nanoparticle sulfidation at 150 mV overpotential. Solution conditions and filter/acquisition rate are similar to those described in Figure 1 caption of the main text.

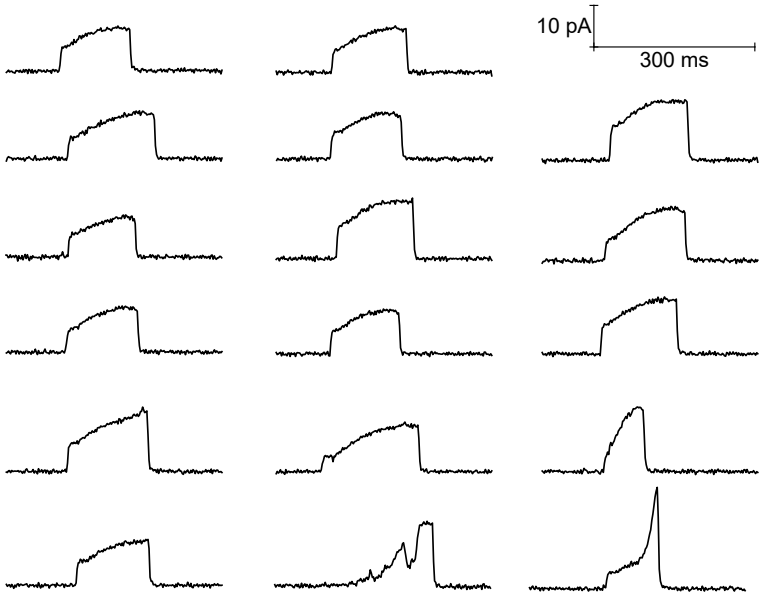

Figure S8. Representative current transients for single-nanoparticle sulfidation at 200 mV overpotential. Solution conditions and filter/acquisition rate are similar to those described in Figure 1 caption of the main text.

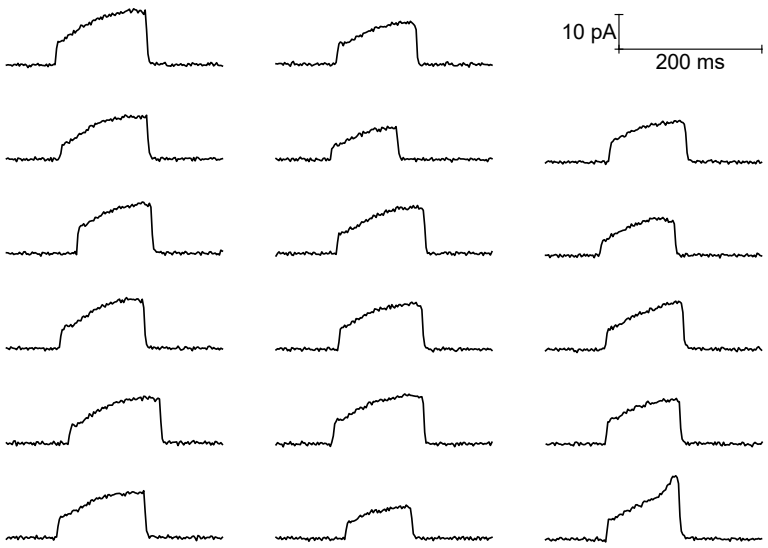

Figure S9. Representative current transients for single-nanoparticle sulfidation at 250 mV overpotential. Solution conditions and filter/acquisition rate are similar to those described in Figure 1 caption of the main text.

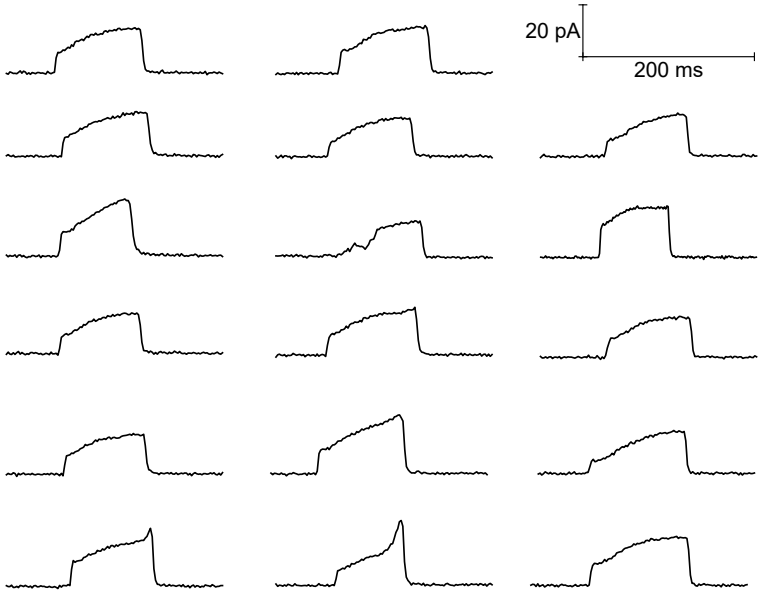

Figure S10. Representative current transients for single-nanoparticle sulfidation at 300 mV overpotential. Solution conditions and filter/acquisition rate are similar to those described in Figure 1 caption of the main text.

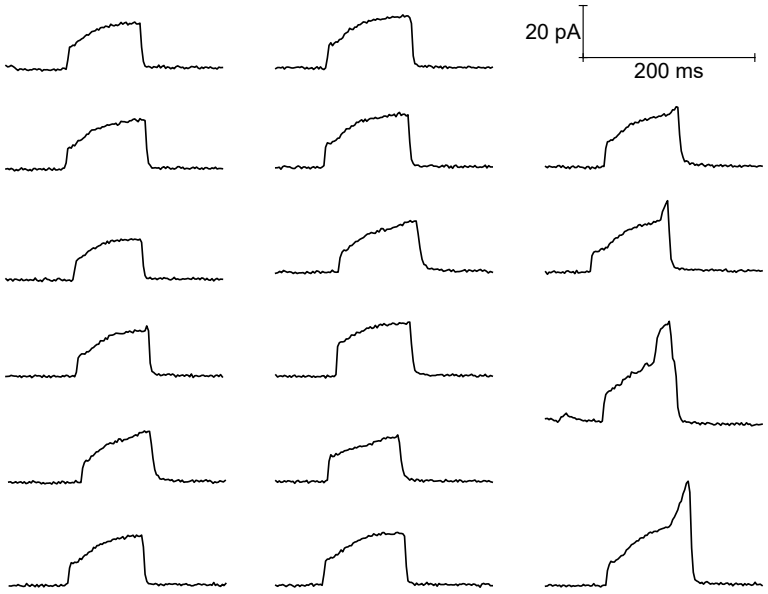

Figure S11. Representative current transients for single-nanoparticle sulfidation at 350 mV overpotential. Solution conditions and filter/acquisition rate are similar to those described in Figure 1 caption of the main text.

S4. Statistical Analysis of Ag Oxidation Charge

Table S1. Measured Ag Oxidation Charge at Varied Overpotentials

E / V	*N*	Q_{mean} / pC	*SD* / pC	*SEM* / pC
0.05	30	1.428	0.319	0.058
0.10	135	1.323	0.338	0.029
0.15	123	1.223	0.340	0.031
0.20	199	1.323	0.356	0.025
0.25	135	1.274	0.310	0.027
0.30	193	1.298	0.326	0.023
0.35	214	1.336	0.407	0.028

Table S2. ANOVA analysis, Variation of Mean *Q* at Different Potentials (Excluding *E* = 0.05 V)

Source of Variation	*SS*	*DF*	*MS*	*F*	*P-value*
Between Groups	1.28E-6	5	1.16E-26	2.0585	0.06831
Within Groups	1.23E-4	993	3.07E-25		
Total	1.24E-4	998			

SD, standard deviation; *SEM*, standard error of the mean; *SS*, sum of squares; *DF*, degrees of freedom; *MS*, mean squares; *F* is ratio of *MS* between groups divided by *MS* within groups. *P-value* represents the probability that the variance among *Q* is not statistically significant.

The *P-value* of 0.068 from Table S2 signifies that we *cannot* reject the null hypothesis at 95% confidence level ($\alpha = 0.05$).

Table S3. ANOVA analysis, Variation of Mean *Q* at Different Potentials (Including *E* = 0.05 V)

Source of Variation	*SS*	*DF*	*MS*	*F*	*P-value*
Between Groups	1.74E-6	6	2.90E-7	2.3473	0.02947
Within Groups	1.26E-4	1022	1.23E-7		
Total	1.28E-4	1028			

The *P-value* of 0.029 in Table S3 signifies that we *can* reject the null hypothesis at 95% confidence level ($\alpha = 0.05$). The average charge measured for the 0.05 V condition may be significantly different from

the mean values measured at higher overpotentials. However, the value of Q_{mean} obtained for the 0.05 V condition is less reliable because of a sample size of only 30 particles, so we cannot conclude whether or not the lowest overpotential condition leads to the highest amount of Ag oxidized per NP.

Table S4. Two-Sample *t*-Test: Theoretical Charge for Full NP Oxidation vs. Measured *Q*

Dataset	*N*	*Mean* / pC	*SD* / pC	*SEM* / pC	*Median* / pC
Theory	612	1.730	0.545	0.022	1.682
Experiment	1029	1.306	0.353	0.011	1.271
Difference		-0.424		0.022	
Overall	1641	1.464	0.480	0.012	1.379

T-TEST STATISTICS

Variance Condition	*t Statistic*	*DF*	*P-value*
Equal Variance Assumed	-19.1085	1639	6.03E-74
Equal Variance NOT Assumed (Welch Correction)	-17.2085	918.86234	4.83E-58

The *t-Test* statistical analysis in Table S4 indicates that the null hypothesis can be rejected. We thus conclude that the mean charge measured from experiment is significantly lower than the mean charge predicted for full Ag NP oxidation.

S5. Voltammetry and coulometry of sulfide reactions at a polycrystalline Ag electrode

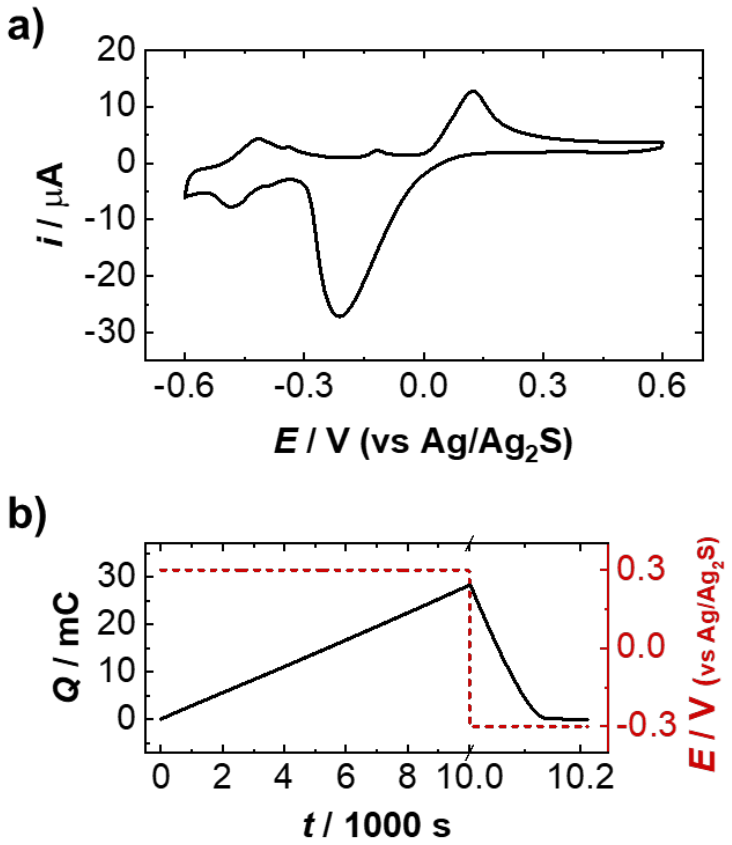

Figure S12. (a) Cyclic voltammogram of sulfide formation and reduction at a polycrystalline Ag electrode, 2 mm diameter, 100 mV s^{-1} scan rate. **(b)** Chronocoulometric trace for anodic Ag_2S formation at 0.3 V for a period of 10,000 s, followed by a potential step to -0.3 V to drive Ag_2S reduction. Deaerated solution contains 1 mM Na_2S and 10 mM NaOH.

S6. Scanning transmission electron microscopy image gallery

E = 0.1 V vs Ag/Ag_2S

Dark field	Bright field	Secondary electron

Particle 1

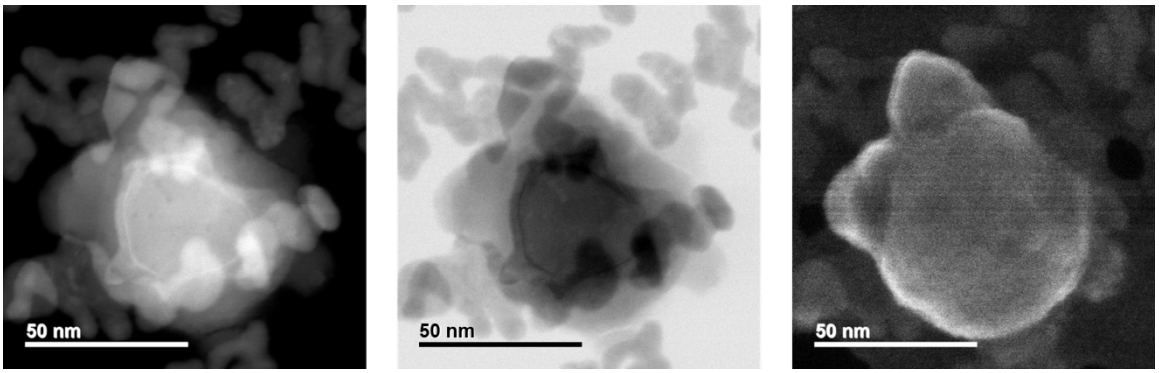

Particle 2

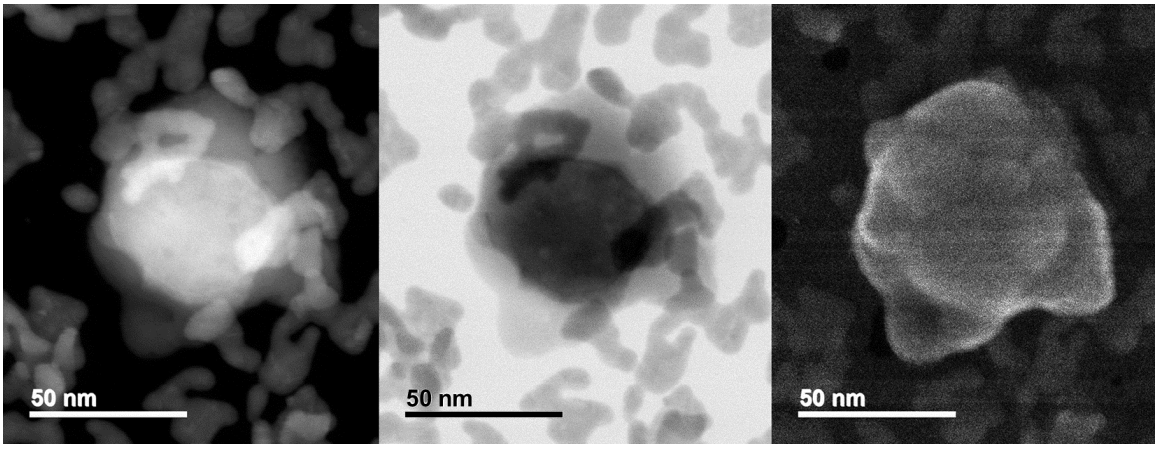

Particle 3

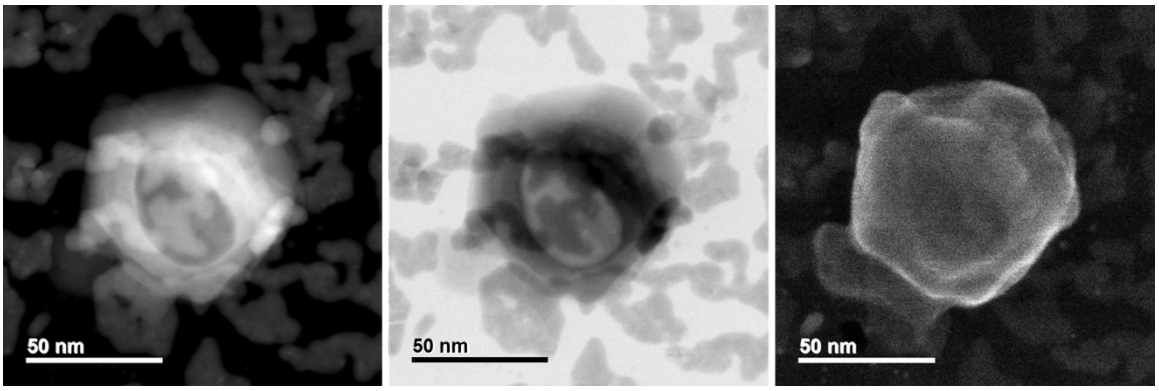

Particle 4

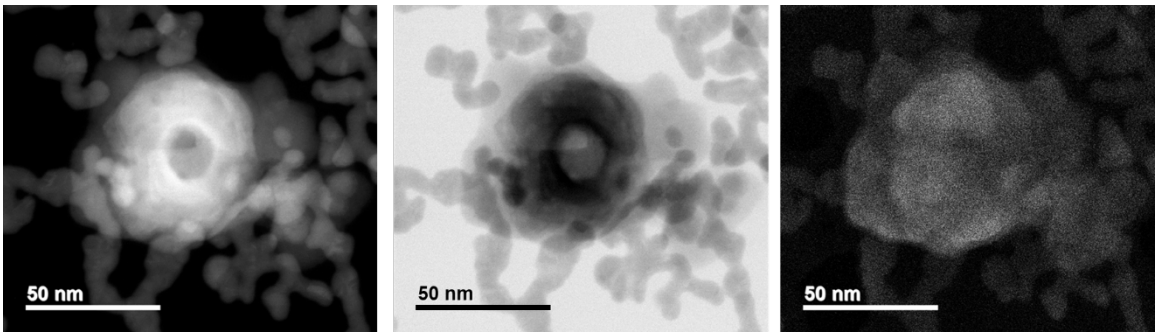

Particle 5

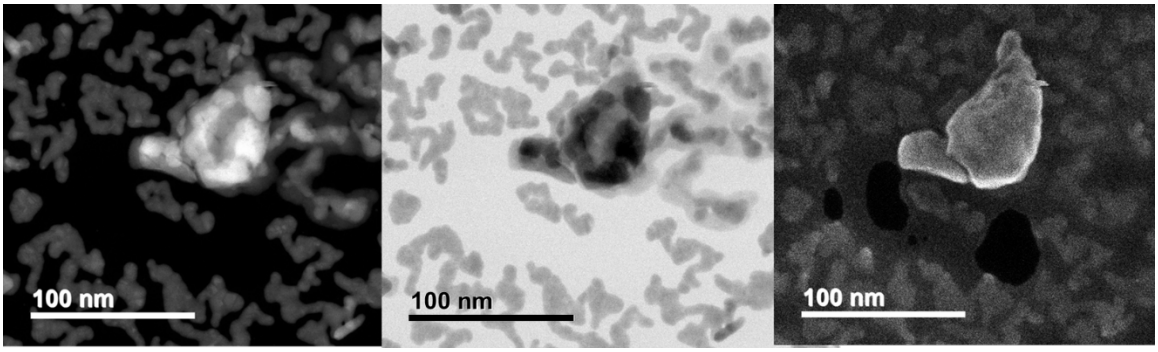

Particle 6

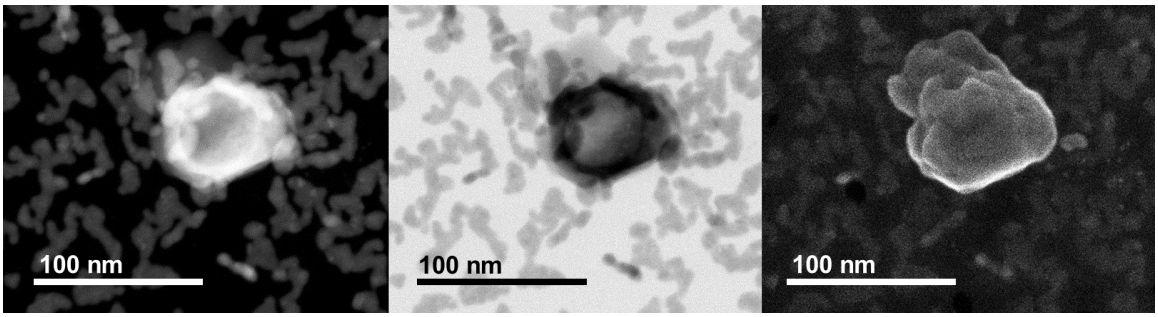

Particle 7

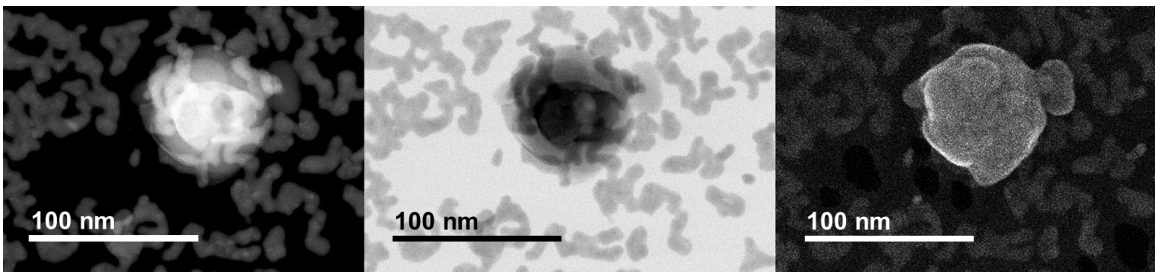

Figure S13. STEM images of seven individual nanoparticles formed by anodic sulfidation of Ag nanoparticles at a gold film coated TEM grid with a 100 mV applied potential vs Ag/Ag_2S. From left to right are dark-field, bright-field, and secondary electron imaging modes.

E = 0.3 V vs Ag/Ag_2S

Dark field **Bright field** **Secondary electron**

Particle 1

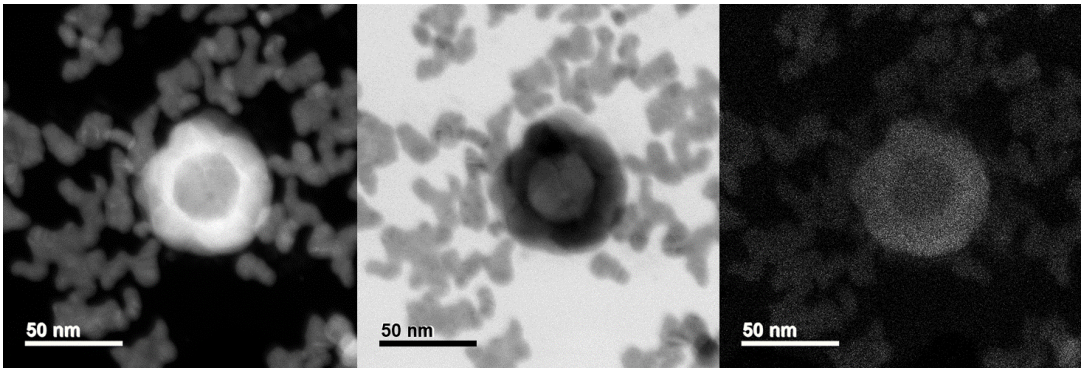

Particle 2

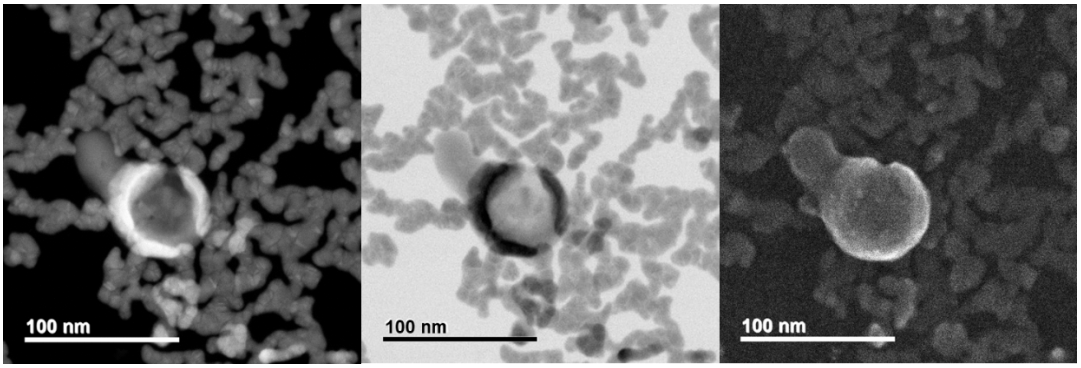

Figure S14. STEM images of two individual nanoparticles formed by anodic sulfidation of Ag nanoparticles at a gold film coated TEM grid with a 300 mV applied potential vs Ag/Ag_2S. From left to right are dark-field, bright-field, and secondary electron imaging modes.

S7. EDX spectral imaging

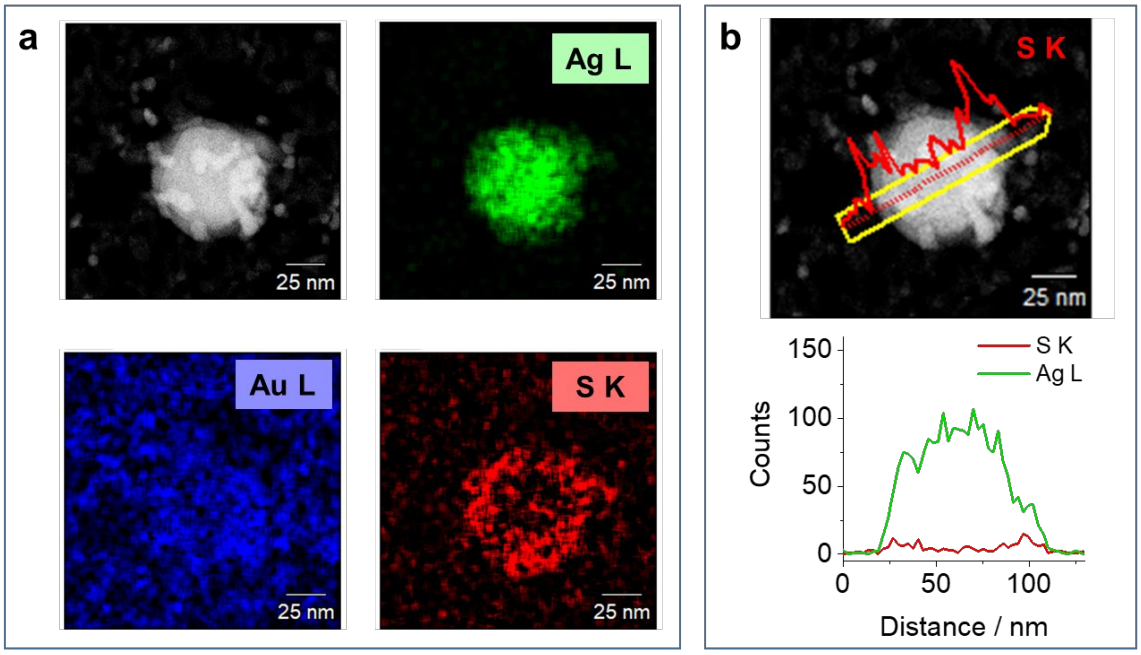

Figure S15. EDX microanalysis of a Ag@Ag_2S nanoparticle formed at 0.1 V overpotential: **(a)** element maps showing Ag, Au, and S; **(b)** linescan of S K counts overlaid with base image (top) and overlay of linescans for S K and Ag L (bottom plot).

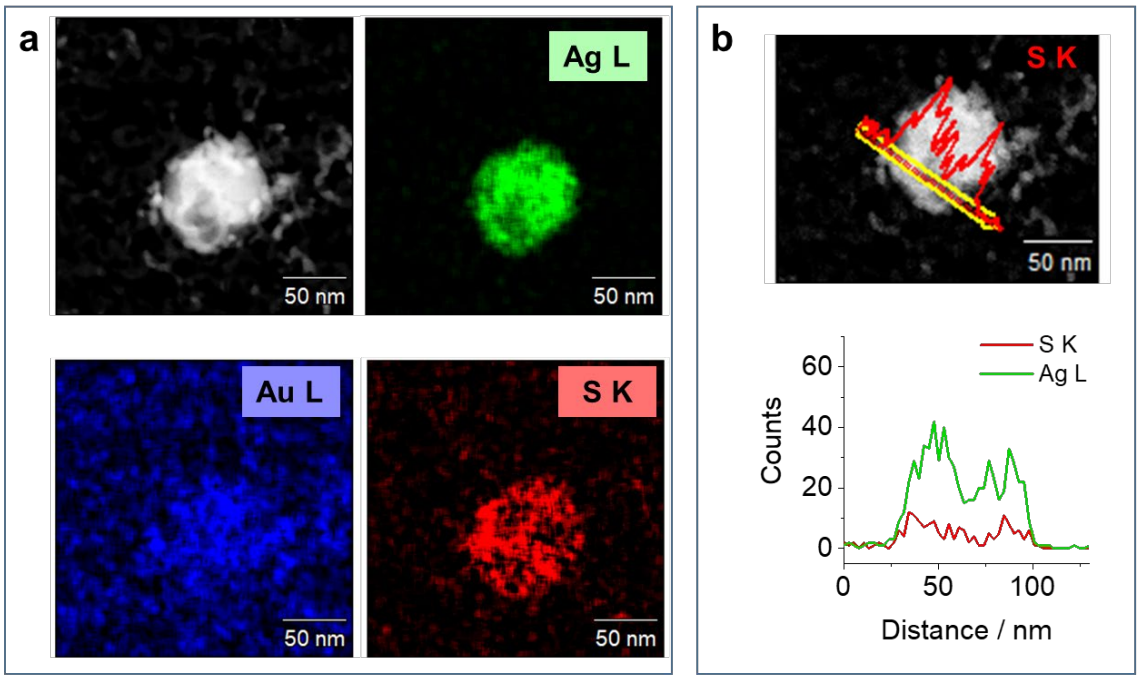

Figure S16. EDX microanalysis of a void-containing Ag@Ag_2S nanoparticle formed at 0.1 V overpotential: **(a)** element maps showing Ag, Au, and S; **(b)** linescan crossing over the void, S K counts overlaid with base image (top) and overlay of linescans for S K and Ag L (bottom plot).

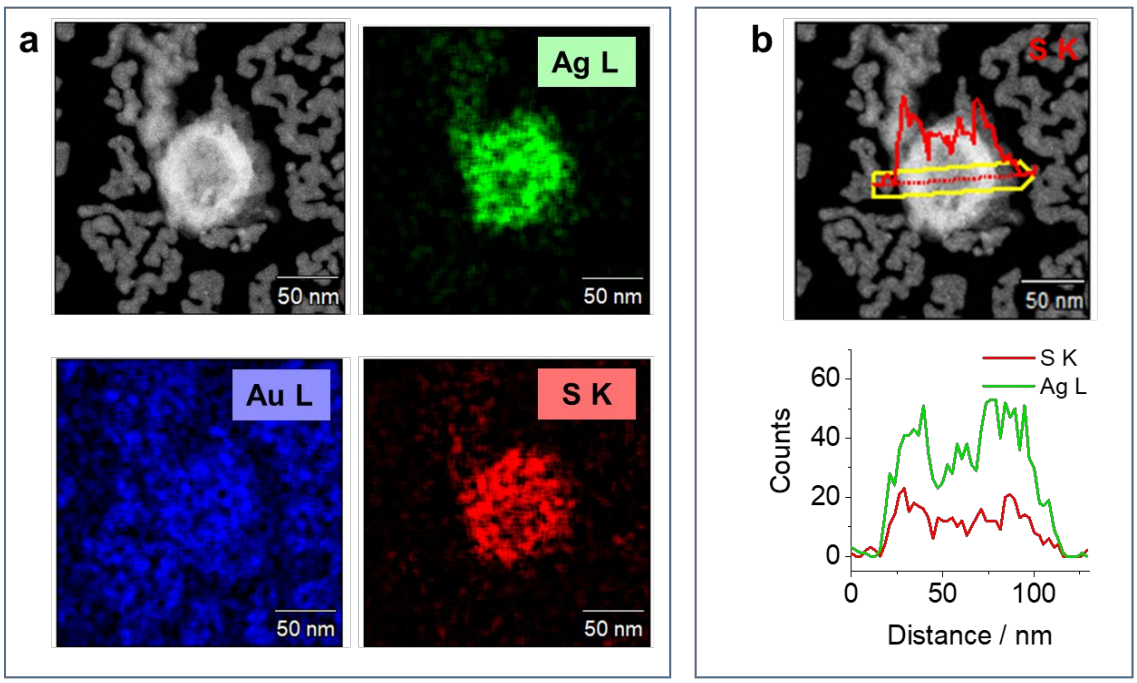

Figure S17. EDX microanalysis of a hollow Ag/Ag_2S nanoparticle formed at 0.3 V overpotential: **(a)** element maps showing Ag, Au, and S; **(b)** linescan crossing over the void, S K counts overlaid with base image (top) and overlay of linescans for S K and Ag L (bottom plot).

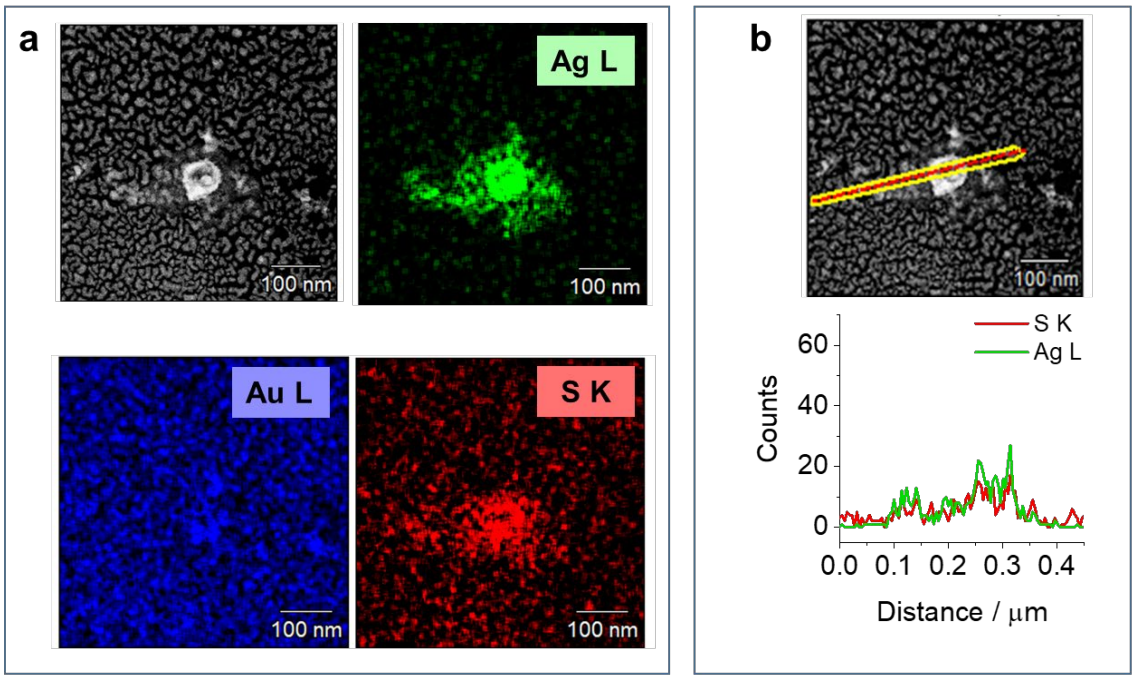

Figure S18. EDX microanalysis of a hollow Ag/Ag_2S nanoparticle formed at 0.3 V overpotential with evidence of Ag_2S precipitation from a transient dissolved species: **(a)** element maps showing Ag, Au, and S; **(b)** linescan extending from neighboring regions at the Au surface and crossing over the particle (top) and overlay of linescans for S K and Ag L (bottom plot).

S8. Calculation of core@shell dimensions from measured Ag oxidation charge

The average volume of a Ag nanoparticle, V_{AgNP}, was calculated from the average diameter measured by TEM, d_{AgNP} (70 nm).

$$V_{\mathrm{AgNP}} = \pi d_{\mathrm{AgNP}}^3 / 6 \quad \text{(S1)}$$

The average volume of Ag oxidized during Ag_2S formation was calculated from the measured faradaic charge, Q (1.3 pC).

$$V_{\mathrm{AgOx}} = \frac{QM_{\mathrm{Ag}}}{n_1 F \rho_{\mathrm{Ag}}} \quad \text{(S2)}$$

M_{Ag} is the molar mass of Ag (107.87 g/mol), ρ_{Ag} is the density of Ag (10.49 g/cm^3), and n_1 is the number of electrons transferred per atom of Ag oxidized (n_1 = 1). The volume of Ag remaining, V_{c}, is thus the volume of the Ag core for the Ag@Ag_2S NP produced,

$$V_{\mathrm{c}} = V_{\mathrm{AgNP}} - V_{\mathrm{AgOx}} \quad \text{(S3)}$$

and the diameter of the Ag core, d_{c}, is $d_{\mathrm{c}} = \left(6V_{\mathrm{c}} / \pi\right)^{1/3}$. (S4)

Combining eqs 1-4 and Q = 1.3 pC, the average Ag core diameter is 42.0 nm.

To solve for the Ag_2S shell thickness, we first evaluate the volume of Ag_2S formed, V_{s}.

$$V_{\mathrm{s}} = \frac{QM_{\mathrm{Ag_2S}}}{n_2 F \rho_{\mathrm{Ag_2S}}} \quad \text{(S5)}$$

Here, $M_{\mathrm{Ag_2S}}$ is the molar mass of Ag_2S (247.80 g/mol), $\rho_{\mathrm{Ag_2S}}$ is the density of Ag_2S (7.23 g/cm^3), and n_2 is the number of electrons transferred to form one Ag_2S unit (n_2 = 2). The average total volume of a Ag@Ag_2S NP, V_{cs}, is simply the sum of the core and shell volumes.

$$V_{\mathrm{cs}} = V_{\mathrm{c}} + V_{\mathrm{s}} \quad \text{(S6)}$$

It follows that the total diameter of the Ag@Ag_2S NP, d_{cs}, is

$$d_{\mathrm{cs}} = \left(6V_{\mathrm{cs}} / \pi\right)^{1/3} \quad \text{(S7)}$$

which gives an average total Ag@Ag_2S NP diameter of 80.4 nm.

The Ag_2S shell thickness, l_{s}, is simply the difference between the radius of the whole Ag@Ag_2S NP and the radius of the Ag core.

$$l_{\mathrm{s}} = (d_{\mathrm{cs}} - d_{\mathrm{c}}) / 2 \quad \text{(S8)}$$

We then calculate an average shell thickness of 18.8 nm.

For nanoparticles containing voids, the average void volume estimated from TEM measurements, V_{v}, was incorporated into the calculation, replacing eq S6 with eq S9.

$$V_{\mathrm{cs}} = V_{\mathrm{c}} + V_{\mathrm{s}} + V_{\mathrm{v}} \quad \text{(S9)}$$

S9. References

1. Lilienfeld, S.; White, C. E., A study of the reaction between hydrogen sulfide and silver. *J. Am. Chem. Soc.* **1930,** *52* (3), 885-892.

2. Elechiguerra, J. L.; Larios-Lopez, L.; Liu, C.; Garcia-Gutierrez, D.; Camacho-Bragado, A.; Yacaman, M. J., Corrosion at the Nanoscale: The Case of Silver Nanowires and Nanoparticles. *Chem. Mater.* **2005,** *17* (24), 6042-6052.

3. Robinson, D. A.; Edwards, M. A.; Ren, H.; White, H. S., Effects of Instrumental Filters on Electrochemical Measurement of Single-Nanoparticle Collision Dynamics. *ChemElectroChem* **2018,** *5* (20), 3059-3067.

4. Gupta, A. Monitoring Progressive Damage Development in Laminated Fiber Reinforced Composite Materials. PhD Thesis, Virginia Tech, Virginia Tech, 2017.

5. Gupta, A., *https://bitbucket.org/arnabocean/public-matlab/src/9abeedd2166c76048447dbfeb55ffcae01b23d96?at=default [BesselFilter.m]*

6. Gao, X.; Zhang, Y.; Weaver, M. J., Adsorption and electrooxidative pathways for sulfide on gold as probed by real-time surface-enhanced Raman spectroscopy. *Langmuir* **1992,** *8* (2), 668-672.

7. Lezna, R. O.; de Tacconi, N. R.; Arvia, A. J., Modulated reflectance spectroscopy and voltammetry of the sulphide/gold system. *J. Electroanal. Chem. Interfacial Electrochem.* **1990,** *283* (1), 319-336.